Journal of Drug Delivery Science and Technology 112 (2025) 107280

Contents lists available at ScienceDirect

Journal of Drug Delivery Science and Technology

journal homepage: www.elsevier.com/locate/jddst

A dual-strategy nanomicelle based on starvation therapy for enhancing tumor immunogenicity

Yuhan Fu [a,b], Sisi Yan [a,b], Jialin Sun [c], Jianchang Huang [a,b], Chunyu Yang [d], Weinan Li [a,b,*], Yanhong Wang [a,b,**]

[a] School of Pharmacy, Heilongjiang University of Chinese Medicine, Harbin, Heilongjiang Province, China
[b] Key Laboratory of Basic and Application Research of Beiyao (Heilongjiang University of Chinese Medicine), Ministry of Education, Harbin, Heilongjiang Province, China
[c] Department of medicine, Heilongjiang Minzu College, Harbin, Heilongjiang Province, China
[d] Department of Pathology, Harbin 242 Hospital, Harbin, Heilongjiang Province, China

ARTICLE INFO

Keywords:
Glucose oxidase
Tumor
Starvation therapy
Immunogenicity

ABSTRACT

Immune checkpoint inhibitors (ICIs) have revolutionized cancer treatment, but their efficacy is limited in the immunosuppressive tumor microenvironment. Immunogenic cell death (ICD), characterized by the release of damage-associated molecular patterns (DAMPs), has the potential to augment anti-tumor immunity and enhance ICI efficacy. However, singular ICD inducers often fail to elicit robust immune responses. To address this limitation, we have developed a pH-sensitive nanomicelle, RPG NMs, co-delivering glucose oxidase (GOx) and resveratrol (Res) to induce ICD in tumor cells. Both Res and GOx retain their stability and bioactivity following encapsulation within the nanomicelles. Under acidic lysosomal conditions in tumor cells, protonated nanomicelles release GOx and Res. GOx lowers the pH, accelerating Res release and enhancing Res-induced ICD via reactive oxygen species (ROS) production. In vitro results indicate that RPG NMs not only consistently achieve starvation therapy (ST) and release ROS, but also effectively inhibit tumor cell activity. Moreover, the nanocmicells significantly induced ICD formation in tumor cells and matured dendritic cells (DCs). RPG NMs integrates ST and ICD to provide a new nano-delivery platform for cancer therapy with dual-strategy sensitizing immunotherapy.

1. Introduction

Malignant tumors pose a significant threat to human health, making the development of effective cancer treatments urgently needed. Immunotherapy with immune checkpoint inhibitors (ICIs), such as anti-PD-1/L1 antibodies, has revolutionized the paradigm of cancer treatment [1]. However, the low response rate of ICIs in immunosuppressive cancers impedes immunotherapy's progress [2]. The immunogenic cell death (ICD) can activate the immune microenvironment, enhancing ICI efficacy by releasing damage-associated molecular patterns (DAMPs), boosting tumor antigenicity, and stimulating the anti-tumor immune system [3]. By activating innate immunity, increasing tumor immunogenicity, and promoting T cell infiltration, ICD synergistically enhances the therapeutic effect of ICIs and helps overcome immune evasion [4]. Among them, anthracycline chemotherapy drugs can induce ICD but cause significant adverse reactions like cardiotoxicity and myelosuppression, affecting patients' quality of life [5]. A single ICD inducer struggles to elicit a robust immune response [6,7].

To address these challenges, various therapeutic strategies have been employed to enhance the tumor immune response [8]. Inducing ICD via endoplasmic reticulum (ER) stress is one such approach [9]. ICD in tumor cells can be induced by ER stress. Upon ER stress, Calreticulin (CRT) relocates to the tumor cell membrane, acting as an "eat me" signal to enhance phagocyte recognition and trigger ICD. Glucose oxidase (GOx)-mediated catalytic reactions generate substantial reactive oxygen species (ROS) and induce hypoxia, both of which are hallmarks of an effective starvation therapy (ST) strategy [10]. Importantly, hypoxia and ROS generation significantly augment ER stress, thereby inducing ICD [11]. Additionally, resveratrol (Res), which modulates mitochondrial function to induce ER stress, has been confirmed to elicit ICD in

* Corresponding author. Heilongjiang University of Chinese Medicine, No. 24, Heping Road, Harbin, 150040, China.
** Corresponding author. Heilongjiang University of Chinese Medicine, No. 24, Heping Road, Harbin, 150040, China.
E-mail addresses: lwnhljucm@163.com (W. Li), wang.yanhong@163.com (Y. Wang).

https://doi.org/10.1016/j.jddst.2025.107280
Received 4 April 2025; Received in revised form 6 July 2025; Accepted 14 July 2025
Available online 15 July 2025

cancer cells [12].

GOx-mediated ST exerts antitumor effects not merely through nutrient deprivation-induced cytotoxicity, but more significantly by intensifying ER stress. When combined with Res, this approach synergistically triggers robust ICD. Importantly, this cooperative mechanism achieves potent immunostimulation without the DNA damage-associated immunosuppressive side effects characteristic of conventional ICD inducers [13,14]. Consequently, GOx-mediated ST can potentiate the Res-induced ICD effect, facilitating a synergistic dual-strategy treatment. However, Res exhibits poor stability and low bioavailability, while GOx, being a protein, is susceptible to degradation in harsh conditions.

Nanomicelles delivery systems address the aforementioned challenges. For instance, nanomicelles like paclitaxel polymer micelles have been developed for clinical tumor treatment [15]. Nanomicelles with hydrophobic cores can effectively encapsulate drugs with poor solubility, thereby solving the problem of Res in its in vivo delivery. GOx, with an isoelectric point of 4.9, carries a negative charge in healthy tissues, allowing it to be tightly adsorbed onto cationic micelles [16]. The pH-sensitive micelles can respond specifically to the acidity of lysosomes in tumor cells to achieve drug release in tumor cytoplasm. Moreover, GOx can reduce local acidity, facilitating the degradation of pH-sensitive micelles and the release of Res.

Herein, we developed co-loaded GOx and Res nanomicelles (RPG NMs) to induce ICD and enhance tumor immunogenicity (Scheme 1). The cationic and pH-sensitive PP copolymer nanocarrier facilitates encapsulation of Res via hydrophobic interactions and adsorption of negatively charged GOx, enabling co-delivery to tumors. RPG NMs exhibit satisfactory stability and biosafety. In the acidic tumor microenvironment, GOx catalysis accelerates Res release with high efficiency. RPG NMs significantly inhibit tumor cell growth, increase DAMPs release, and promote DCs maturation. Thus, RPG NMs could activate the immune response and serve as a novel ICD inducer for immunotherapy. Therefore, RPG NMs can initially activate the immune response, which has the potential of ST and ICD dual-strategy synergistic sensitization immunotherapy.

2. Materials

Res, GOx and 3500 kDa dialysis bag were from Yuanye (Shanghai, China). Coumarin 6 was from Luoen (Shanghai, China). Phosphate buffer (PBS) was from Saiweier (Shanghai, China). Pyrene probe was from Merk (Shanghai, China). H_2O_2 detection kits and BCA content determination kits were from BaiqiaoBio (Shanghai, China). Adenosine triphosphate (ATP) content activity assay kit was from Grace Biotechnology Co., Ltd (Suzhou, China). Phosphotungstic acid negative staining solution was from Beijing Solarbio Science & Technology Co., Ltd (Beijing, China). 1640 medium was from BaiDi Biotechnology Co., Ltd. (BDBIO) (Hangzhou, China). The microwell plates were from CellPro Biotechnology Co., Ltd. (Suzhou, China). The CCK-8, ROS assay kit, H_2O_2 detection kit, BCA content determination kit and DAPI were from Biyuntian (Beijing, China). JC-1 mitochondrial membrane potential

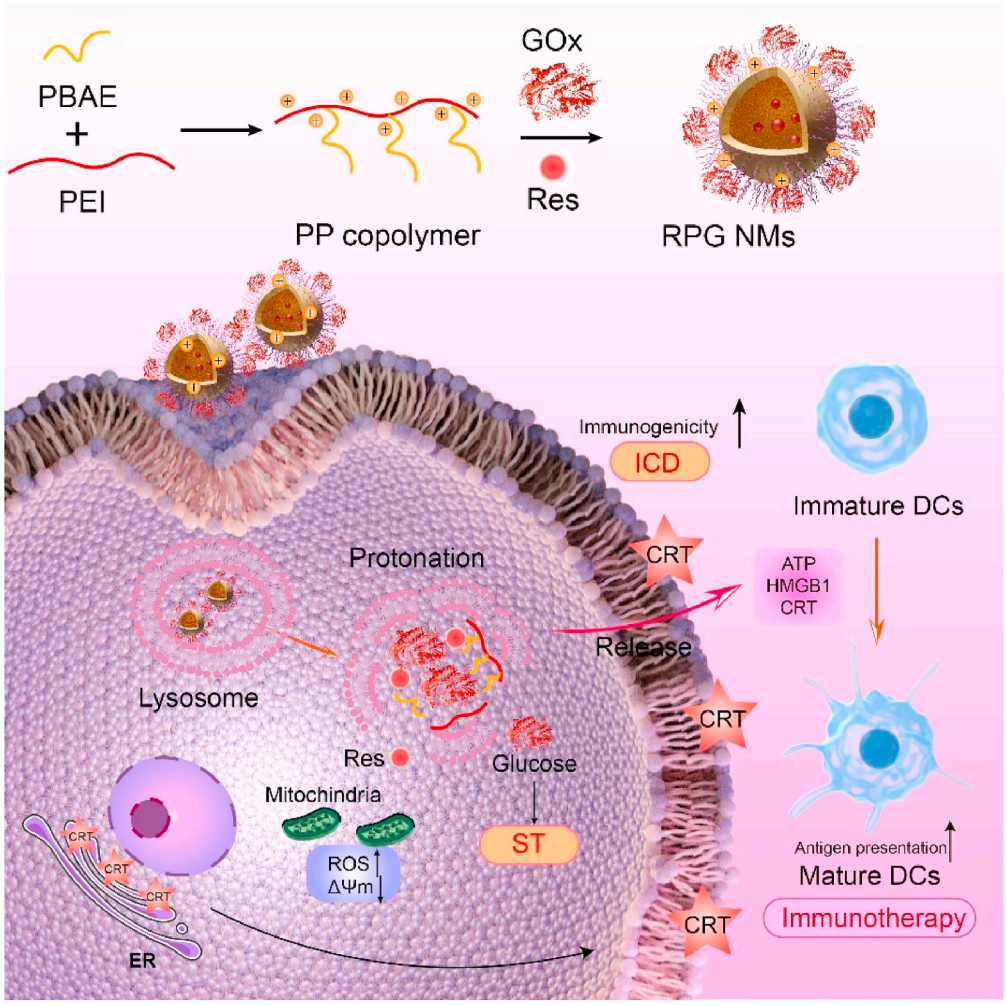

Scheme 1. RPG NMs were constructed by loading Res and GOx through self-assembly behavior. After entering tumor cells, RPG NMs consumed a large amount of glucose to achieve ST. Subsequently, RPG NMs triggered ICD in tumor cells and lead to the maturation of DCs.

detection Kit was form Wanrui (Beijing, China). GM-CSF and IL-4 were from MCE (Shanghai, China). Cell cryopreservation solution was from Seven/Abcells (Beijing, China). The confocal culture dish (1050001) was from SAINING Biotechnology (Suzhou, China). Cell cryopreservation tubes were from NEST Biotechnology Co. Ltd. (Wuxi, China). The Phosphate Buffered Saline (PBS) was from Saiweier Biotechnology (Wuhan, China). The Fetal bovine serum (FBS) was from Cellmax (SA311.02) (Beijing, China). The High Mobility Group Box 1 (HMGB1) Elisa kit (JL51819-96 T) was from JONLNBIO (Shanghai, China). Calretinin Rabbit pAb was from Zen bioscence (Chengdu, China). Goat anti-rabbit IgG (H + L) antibody was from Huamei (Shanghai, China). APC labled-CD11c, FITC labled-CD80 and PE labled-CD86 were from ABclonal (Shanghai, China).

The Bone Marrow-Derived Dendritic Cells (BMDCs) were obtained from mouse tibial bone marrow stem cells after induced differentiation. The culture conditions were as follows: the obtained bone marrow cells were spread into a 6-well culture plate, and 1640 medium containing GM-CSF (25 ng/mL) and IL-4 (10 ng/mL) was added. The cells were incubated at 37 °C in a 5 % CO_2 incubator. The medium was partially changed on the second and fourth days and supplemented with cytokines in the culture medium.

CT26. WT cells were form Procell (Hubei, China). Cells were cultured in 1640 medium containing 10 % FBS. When the cells reached 80 % density, they were digested with trypsin and passaged. Some of the cells could be frozen by cryopreservation. The passaged cells should be exchanged for medium on the second day to ensure a clean growth environment.

3. Method

3.1. Preparation of micelles

The composite PP of polyβ-amino ester (PBAE) and polyethyleneimine (PEI) was previously prepared in our laboratory. In brief, the preparation method of RPP NMs employed the organic solvent evaporation method. 100 mg of the PP copolymer was dissolved completely in 1 mL of methanol using ultrasound. 20 mg of Res was weighed and dissolved in 1 mL methanol, and the above solution was mixed as the organic phase, which was then slowly dropped into 50 mL water at pH 7.4. At 25 °C and 1000 rpm, the sample was stirred for 3 h using the magnetic stirrer (MS-S, DLAB Scientific Co., Ltd, China). Finally, the solution was filtered through a 0.22 μm filter to remove impurities. Then, the RPP NMs solution was ready. For the cell uptake experiment, free C6 was used to replace Res, and C6/PP NMs were prepared under the same conditions.

Moreover, the loading mode of GOx is electrostatic adsorption. 10 mg of GOx was dissolved in 2 mL of pH 7.4 PB S. It was added dropwise to the RPP NMs or PP NMs solution, and the RPG NMs or GPP NMs solution was obtained after being balanced at 25 °C with dark stirring for 2 h. Among them, RPP is the micelle loaded solely with Res. GPP is the micelle loaded solely with GOx.

3.2. Characterization of the micelles

The 0.012 mg/mL solution of pyrene was prepared and placed in ampoules. The acetone in the bottles was then blown dry with nitrogen. 50 mg PP was dissolved in 10 mL double steaming water, and gradient dilution was made into PP solutions of different concentrations. Each solution was placed in a bottle containing acetone and incubated at 60 °C for 6 h. The samples were taken out and measured with a fluorescence spectrophotometer (RF-6000, SHIMADZU, Japan). The ratio of fluorescence intensity at 384 nm and 373 nm wavelengths (I_{384}/I_{373}) was calculated, and the ratio was plotted together with the concentration of PP to determine the critical micelle concentration (CMC) value.

The average particle size, particle size distribution, polydispersion coefficient (PDI) and zeta potential of NMs were measured by Particle size instrument (Zetasizer Nano ZS90 instrument, Malvern, UK). The RPG NMs solution was diluted tenfold with double-distilled water, and subsequently, aliquots were introduced into the particle size cell and the zeta potential cell for the measurement of particle size and zeta potential, respectively. The morphology was measured after the RPG NMs solution was stained negatively with 2 % phosphotungstic acid negative staining solution. The morphology of RPG NMs was characterized by transmission electron microscopy (TEM, JEM-1200EX, Hitachi, Japan).

The encapsulation rate (EE) and drug loading (LC) of Res in RPP NMs were determined by HPLC (LC-20AD, SHIMADZU, Japan). 5 mL RPP NMs solution was added to methanol and demulsified with ultrasonic crusher. The total content of Res in demulsification solution was determined by HPLC and recorded as M_1. 5 mL of RPP NMs solution was taken and centrifuged in ultrafiltration centrifuge tube (3000 mw) at 10,000 rpm for 30 min. The resulting supernatant was measured by HPLC for the amount of free Res M_2. M_3 is the mass of carrier PP. The encapsulation efficiency (EE) and loading capacity (LC) were calculated according to the formula:

$$EE\% = \left(\frac{M_1 - M_2}{M_1}\right) \times 100\%$$

$$LC\% = \left(\frac{M_1 - M_2}{M_1 - M_2 + M_3}\right) \times 100\%$$

The loading rate of enzyme GOx was measured by BCA assay. The RPG NMs solution prepared by 10 mL was centrifuged at 15,000 rpm for 1 h, and the concentration of free GOx was measured as Cf in the supernatant. Among them, Cf and Cs are the concentration of free GOx and the total concentration of GOx, respectively, and W1 is the mass of the carrier PP. The Loading Efficiency (LE) and Loading Faculty (LF) of GOx were calculated using the following formula:

$$LE\% = 1 - \frac{C_f}{Cs}$$

$$LF\% = \frac{C_f}{C_s + W_1}$$

3.3. External release experiment

The release behavior of Res in RPG NMs was investigated by dialysis method. Typically, 10 mL of free Res and RPG NMs are added to a 3500 kDa dialysis bag. The medium release conditions were pH 7.4, pH 5.5 + glucose, and pH 5.5 - glucose, respectively. Then, the dialysis bag was placed in 100 mL dialysis medium prepared with PBS and oscillated in a constant temperature shaker at 37 °C and 80 rpm for 48 h. Each dialysis medium contains 1 % Tween 80 to facilitate the dissolution of Res. The Res content of the sampled solution was determined by HPLC.

The release behavior of GOx in RPG NMs was investigated by dialysis. The free GOx and RPG NMs were placed into centrifuge tubes under different conditions. The experiment was performed under the same conditions as above. Sample 1 mL at each time point and add equal volume of release medium. The sample solution was centrifuged at 15,000 rpm for 10 min, and the supernatant was taken to determine the concentration of GOx with the BCA protein concentration kit. The cumulative release rate (Er) of the Res and GOx was calculated according to the formula:

$$E_r = \frac{V_e \sum_{1}^{n-1} C_i + V_0 C_n}{m_{drug}}$$

The meaning of each variable in this formula: E_r: cumulative drug release; V_e: release medium displacement volume; V_0: total volume of releasing medium; C_i: the concentration of the sample release at the i replacement; m_{drug}: total quality of drug input; n: the number of times of the replacement releases the medium.

3.4. Stability of NMs in serum

RPG NMs was mixed with PBS containing 10 % bovine serum and incubated in a constant temperature shaking table at 37 °C for 48 h 1 mL was sampled from the solution at 0, 6, 12, 24, 36, 48 h, respectively, and the particle size and PDI values were determined by Particle size instrument.

3.5. Enzyme activity assay

The effects of catalytic reaction induced by GOx on tumor pH and H_2O_2 concentration were investigated. The RPG NMs solution containing 1 mg/mL GOx was dropped into the pH 5.5 PB S solution containing glucose. Then, the pH of the solution was determined at different times. According to the H_2O_2 detection kit, the absorbance was measured at 570 nm with the Microplate Reader (Varioskan ALF, Thermo Fisher Scientific, USA).

In order to compare the catalytic performance of RPG and free GOx, different concentrations of glucose were set for the study. 1 mL of 1 mg/mL RPG NMs solution and 1 mg/mL of free GOx were dropped into PBS solution containing 0, 0.5, 1, 2, 3, and 4.5 mg/mL glucose at pH 5.5, respectively. After 2 h, the pH changes and H_2O_2 concentration were measured.

3.6. Determination of hemolysis

Blood was collected from the orbital venous plexus of mice and placed into an anticoagulant tube. Then, the precipitate was obtained by centrifugation at 4500 rpm for 10 min and washed three times with normal saline until the supernatant was clarified. The precipitate was diluted with normal saline to prepare erythrocyte suspension. 20 μL was added to a centrifuge tube containing 980 μL RPG NMs of different concentrations, distilled water (positive group), and normal saline (negative group). The samples were incubated at 37 °C for 2 h, centrifuged, and photographed to observe the hemolysis, and the absorbance value at 570 nm was determined by microplate reader. The hemolysis rate of RPG NMs was calculated according to the formula:

$$\text{Hemolysis}\% = \frac{A_x - A_n}{A_p - A_n} \times 100\%$$

where, Hemolysis is the RBC hemolysis rate, and A_x, A_n and A_p are the absorbance values of each preparation group, negative control group and positive control group, respectively.

3.7. Cellular uptake

To evaluate the ability of the PP to promote tumor cell uptake, C6 was used as a fluorescent model drug. CT26 cells were incubated in 12-well plates at a density of 2.5×10^4 cells/well for 24 h. The medium diluted C6/PP NMs with free C6 solution were added and incubated for 1 h, 2 h, and 3 h. The original supernatant was removed and washed three times with cold PBS. Then, cells were fixed with 4 % paraformaldehyde for 10 min and incubated with DAPI dye for 10 min. After washing three times with PBS, the cells were placed under a fluorescence microscope to observe the luminescence. Uptake behavior was quantified by flow cytometry (FongCyte™, Challen Biotechnology, Beijing).

3.8. Cell viability

The cell viability was detected by CCK-8 method, and the cells were seeded into 96-well plate at a density of 5×10^3 cells/well and cultured for 24 h. In PP NMs group, 0, 100, 200, 400, 600, 800, and 1000 μg/mL PP were used to prepare blank medium and incubate cells, respectively. Res in the Free Res, RPP NMs and RPG NMs groups were prepared into drug containing medium with concentrations of 0, 53, 30, 22.5, 16.87, 11.25 and 5.62 μg/mL. The GPP NMs group and RPG NMs group were prepared with drug-containing medium with GOx concentrations of 0, 21.87, 43.75, 87.5,175, 350, and 700 ng/mL, which were divided into glucose free and glucose containing conditions. They were added to different culture Wells and incubated for 24 h. After that, the original drug containing medium was removed, and 20 μL of CCK8 solution was added and incubated for 1 h. The wavelength of the microplate reader was adjusted to 450 nm, the absorbance was measured, and the cell survival rate and IC_{50} value were calculated.

3.9. ROS

CT26 cells in logarithmic growth phase were cultured at a density of 5×10^5/well in cell 6-well plates. After cell attachment, GPP NMs, RPP NMs, RPG NMs, and drug-free medium were added to each well. The content of GOx and Res in the single-drug micelle group was equivalent to that in the RPG NMs group. After the cells were treated with the above drugs for 6 h, the diluted DCFH-DA ROS fluorescent probe solution was added, and the ROS production was observed under a fluorescence microscope immediately and quantitative analysis by flow cytometry after 20 min of incubation.

3.10. Mitochondrial membrane potential ($\triangle\Psi m$)

CT26 cells were cultured at 2.5×10^4 cells/well in 12-well plates. Cells were incubated with medium, GPP NMs, RPP NMs, and RPG NMs for 24 h, respectively. The original medium was removed, and the JC-1 staining working solution was added to the blank medium at a 1:1 ratio and incubated for 1 h at 37 °C. After washing three times with JC-1 staining buffer, 1 mL of sterile PBS was added to each well, and the luminescence intensity of red and green was immediately observed under a fluorescence microscope. The Image-J software was used to semi-quantitatively analyze the experimental results.

3.11. ICD inducibility

3.11.1. The release of ATP and HMGB1

CT26 cells were cultured at 2.5×10^4 cells/well in 12-well plates and incubated for 24 h. Cells were incubated with medium, GPP NMs, RPP NMs, and RPG NMs for 24 h, respectively. After centrifugation at 3500 rpm for 5 min, the supernatant was collected and placed into different tubes. The ATP content in the samples was determined according to the instructions in the ATP content determination kit. Similarly, the resulting samples were subjected to the determination of HMGB1 content to determine the amount of HMGB1 released under different administration conditions. According to HMGB1 Elisa kit, the content of HMGB1 in different groups was determined by detecting OD value at 450 nm with a microplate reader.

3.11.2. Expression of CRT and determination of DCs maturity

CT26 cells in logarithmic growth phase were cultured at a density of 5×10^4/well in a cell confocal culture dish and incubated for 24 h at 37 °C in an incubator with 5 % CO_2. After washing three times with PBS, each well was added: GPP NMs, RPP NMs, RPG NMs, and drug-free medium served as control. After 12 h of incubation, the cells were washed using PBS. The plates were fixed with 4 % paraformaldehyde for 10 min and washed three times with PBS. Goat serum was added for blocking for 30 min, and then without washing, the diluted CRT primary antibody was directly added by dropping and incubated overnight in a humidified 4 °C environment. After washing three times with PBST, the diluted secondary antibody with fluorescent labeling was added. Finally, the cells were incubated with DAPI for 10 min and the fluorescence expression was observed under Confocal laser scanning microscope (CLSM) (SP8, Laica, Germany).

BMDCs were obtained from mouse tibial bone marrow stem cells after induced differentiation. CT26 cells were seeded in 12-well plates at

5×10^4 cells/well and cultured overnight. Cells were incubated with medium, GPP NMs, RPP NMs, and RPG NMs for 24 h, respectively. Subsequently, CT26 cell debris was collected by centrifugation. The collected cell debris was co-cultured with BMDCs for 12 h. The cells were stained with antibodies CD11c-APC, CD80-FITC and CD86-PE, and the maturation rate of DCs was analyzed by flow cytometry.

3.12. Statistical analyses

The mensuration was repeated 3 times and the data is reported as mean ± SD (standard deviation). The analysis of laboratory finding was made using GraphPad Prism 11. Statistical analysis was done with a One-way ANOVA analysis of variance, followed by Tukey's post hoc tests for multiple comparisons. Significance at $^*p < 0.05$, $^{**}p < 0.01$ and $^{***}P < 0.001$ were acceptable.

4. Result and discussion

4.1. Characterization of the micelles

CMC is a necessary parameter for the thermodynamic stability of micelle, and a smaller value indicates a stronger stability [17]. It also determines the anti-dilution ability of the micelles after injection to the circulation of blood. In Fig. 1a, the CMC of PP micelles was determined based on the inflection point of the ratio of PP concentration to fluorescence intensity (I_{384}/I_{373}). With the increase of PP concentration in solution, the ratio increased slowly, but an inflection point was observed at LogC = 0.4233 mg/L. The CMC of amphiphilic PP was calculated to be 2.6503 mg/L. CMC values for micelles in the range of 1–5 mg/L ensure stability in the blood environment [18]. This showed the ability of PP micelles to resist fairly strong dilution and thus maintain colloidal stability.

The particle size distribution and TEM morphology of RPG NMs are shown in Fig. 1b and c. The particle size distribution is the distribution curve obtained from three parallel experiments, and the value was 99.32 ± 2.8 nm. The PDI of RPG NMs was 0.19 ± 0.07, and the zeta potential was 4.2 mV. TEM morphology showed that RPG NMs had a size of about 90 nm in the dry state and presented a spheroid-like shape.

The particle size of tumor injection needs to meet certain physiological conditions, mainly the enhanced permeability and retention effect (EPR) effect [19]. The abnormal distribution of blood vessels and cells in tumor tissues leads to enhanced vascular permeability, which promotes the aggregation of 100–800 nm particles in tumors. RPG NMs meet the requirements of EPR effect and have the ability to achieve passive targeting and substantial retention in tumor tissue. Although PEI in PP can carry an abundant positive charge, it is loaded with negatively charged GOx by electrostatic adsorption, resulting in a potential drop. The charge shielding effect of GOx reduces the coagulation of micelles and the occurrence of adverse reactions after the adsorption of a large amount of protein in the blood [20]. At the same time, RPG NMs have a low positive charge, which is conducive to the attraction and internalization of micelle by cancer cell membrane. In RPG NMs, the EE of Res was 13.97 ± 0.23 %, and the LC was 81.16 ± 0.66 %. The LE of GOx in micellar was 69.50 ± 1.21 %, and the LF was 12.20 ± 0.76 %. Therefore, RPG NMs show strong drug loading capacity, which is the basis for the excellent therapeutic effects.

4.2. External release experiment

The release behavior of RPG NMs under tumor simulated conditions (pH 5.5 and pH7.4) was measured. As shown in Fig. 1d, the release rate of free Res was the fastest, reaching 80 % within 12 h. In contrast, RPG NMs at pH 7.4 released an extremely low amount of Res, not exceeding 50 % within 48 h, demonstrating the controlled release of the drug from the micelles. Notably, the release of Res from micelles in pH 5.5 + glucose was faster than that of the group without glucose, with a cumulative release of about 80 % within 20 h. Since the isoelectric point of GOx is 4.2 and the charge of GOx is greatly changed in pH 5.5. The

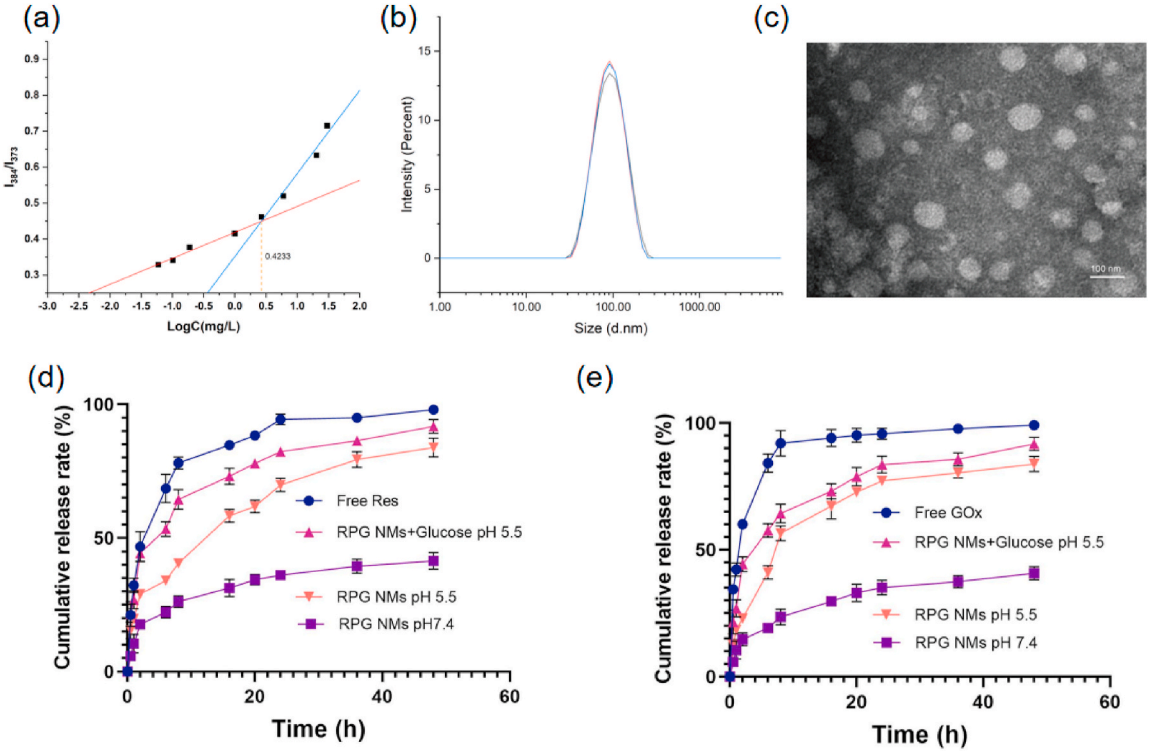

Fig. 1. **(a)** The experimental results of CMC determination, (b) particle size distribution diagram of RPG NMs, (c) morphological characterization of RPG NMs (scale bar = 100 nm), (d) cumulative release rate curves of Res under different conditions, and (e) cumulative release rate curves of GOx under different conditions. n = 3, the data are expressed as the mean ± SD.

positive charge is distributed on the surface, then the electrostatic adsorption force is reduced [21]. Thus, GOx is then released by the micelles and catalyzed. Due to the release of large amounts of gluconic acid from the catalyzed reaction of GOx, the local pH can be rapidly reduced, inducing accelerated depolymerization of micelles and the release of Res. Therefore, GOx facilitated the release of Res from the core of the micelles and improved the efficiency of drug action.

As shown in Fig. 1e, free GOx can be completely released in a short time, but only less than 40 % can be released in pH 7.4. RPG NMs in pH 5.5 conditions containing glucose had the fastest release rate, showing the ability of GOx to be released in large amounts at lysosomal acidity. This result is derived from the fact that PP carriers will be protonated at acidic conditions, showing abundant positive charges, repsing and releasing GOx. At the same time, GOx accelerates the protonation of the carrier and accelerates the release of GOx in the reaction of glucose. In summary, micellar delivery avoids the leakage of Res and GOx in normal tissues and ensures the rapid release of Res and GOx in tumor cells.

4.3. Stability of NMs in serum

Micelles are nano-sized particles formed by the self-assembly of amphiphilic polymers through hydrophobic forces. However, the composition of blood circulation in the body is complex, which is easy to affect the particle size and dispersion of the micelles [22]. Therefore, the stability of micelles in vivo determines the biological safety of the drug. As shown in Fig. 2a, RPG NMs showed small changes in particle size and PDI values within 48 h. The maximum PDI value did not exceed 0.35, indicating that the micelles maintained excellent dispersibility within 48 h. After 24 h, the particle size and dispersibility increased slightly, which may be due to the trace coagulation of proteins and micelles in the serum [23]. Therefore, RPG NMs can maintain stability and safety in blood as an injection.

4.4. Enzyme activity assay

GOx can catalyze the oxidation of glucose to produce gluconic acid and H_2O_2. As shown in Fig. 2b, the catalytic progression of RPG NMs extended with time and reached a plateau around 2 h. To mimic the nutritional condition of tumor cells, 4.5 mg/mL glucose was used as the maximum response concentration. As shown in Fig. 2c, within 2 h, the pH decreased with increasing glucose concentration, and the H_2O_2 concentration gradually increased. The results showed that RPG NMs and free GOx could achieve excellent catalytic effects at tumor cell acidity. Moreover, the rate of H_2O_2 produced by RPG NMs was similar to that produced by free GOx, and the pH change was similar. This result indicates that the delivery of GOx by gelatin micelles almost does not affect its catalytic activity, which is beneficial to the therapeutic effect. The catalytic activity of GOx is optimal at pH 5.5–5.8, which is in line with the acidity of lysosomes in tumor cells [24]. In addition, the most suitable catalytic temperature of GOx is 30 °C–35 °C, which is consistent with the human body temperature. Therefore, GOx is enough to maintain initial activity and exert maximum catalytic effectiveness in micelle.

4.5. Determination of hemolysis

The hemolysis assay of nanomicelles is a key factor in evaluating the biological safety of the preparation. Hemolysis can cause the release of lipid membranes, enzymes, hemoglobin, bilirubin and other substances in erythrocyte, thus affecting the stability and drug activity of the preparation [25,26]. Moreover, an increase in the amount of free hemoglobin in plasma can cause toxic reactions or stress responses in the kidneys and other organs [27]. As shown in Fig. 2d, RPG NMs caused insignificant hemolysis, and the percentage of hemolysis was less than 5 %. The saline and water groups were used as controls for negative and positive results, respectively. The excellent biosafety of RPG NMs was demonstrated by a hemolysis rate of less than 5 % even at a high concentration (4 mg/mL).

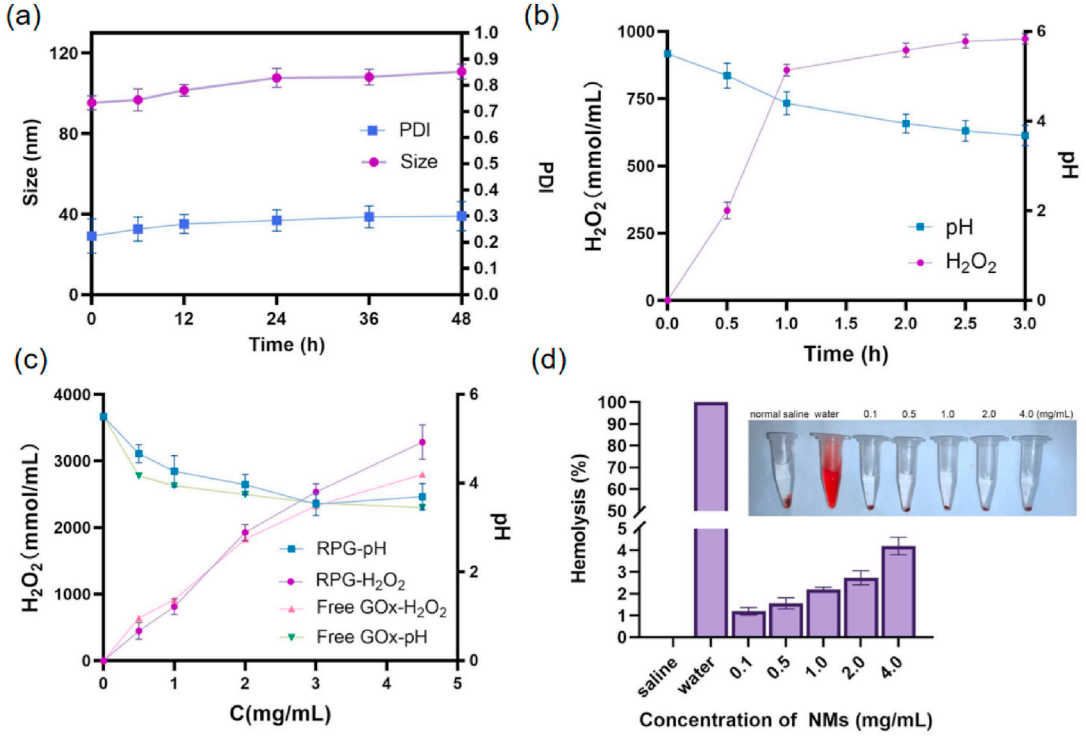

Fig. 2. (a) Stability test results of RPG NMs, (b) H_2O_2 and pH changes of RPG NMs at different times, (c) catalytic efficiency of RPG NMs and free GOx at various glucose concentrations, and (d) hemolytic test results of RPG NMs. n = 3, the data are expressed as the mean ± SD.

4.6. Cellular uptake

The efficiency of micelle uptake by cells is directly related to the therapeutic efficiency of drugs. Fig. 3 shows the phenomenon that the green fluorescence intensity in both Free C6 and C6/PP NMs increased with time. At the same time, the green fluorescence in the C6/PP NMs group was significantly stronger than that in the Free C6 group. As shown in Fig. 4a, at 1 h, 2 h and 3 h, the fluorescence intensity of free C6 was significantly lower than that of NMs group (**$p < 0.01$ and ***$p < 0.001$), indicating the excellent delivery efficiency of NMs for hydrophobic molecules. PP as a carrier could accelerate the process of drug entering cells and improve the efficiency of drug use. The fluorescence intensity of C6/PP NMs at 2 h was twofold greater than that at 1 h. At 3 h, the uptake fluorescence intensity in the NMs group was 4 times higher than that at 1 h, showing rapid cellular internalization behavior. This result is due to the abundant positive charge on the surface of the PP, although some cations are screened by GOx. The membrane surface of cancer cells is thought to have a negative charge that favors the internalization of cationic micelles [28].

4.7. Cell viability

The degree of inhibition of CT26 cells by PP blank micelles and RPG NMs under various conditions was verified. As shown in Fig. 4b, PP was weakly cytotoxic at concentrations from 0 to 1000 μg/mL. Even at a concentration of 800 μg/mL, cell viability remained above 80 %, indicating that PP is biosafe. Fig. 4c showed the activity of CT26 cells with free drug and micelle intervention at Res concentrations. With the increase of Res concentration, the toxicity of both free drugs and micelles increased.

As shown in Fig. 4d, the IC_{50} of free Res was 27.27 ± 2.63 μg/mL. RPP (17.27 ± 5.67 μg/mL) and RPG NMs (11.71 ± 4.46 μg/mL) were more effective in inhibiting tumor cell activity than free Res (*$p < 0.05$). RPG delivered by PP carrier exerts a more significant inhibitory effect than the free drug (21.50 ± 3.74 μg/mL) (*$p < 0.05$). The reason for this phenomenon is that the PP carrier could promote the process of cellular internalization, and more drugs can exert almost all efficacy. The catalytic process of GOx intensified the dissociation process of the PP carrier, accelerated the release of Res and GOx in tumor cells and tumor suppression. Fig. 4e and f showed the toxicity of GPP NMs and RPG NMs to CT26 cells. Under the culture conditions containing glucose, the activity of tumor cells was more likely to be inhibited by GPP or RPG. The IC_{50} values for each group were 302.1 ± 16.28 ng/mL in the GPP + Glucose group, 686 ± 20.88 ng/mL in the GPP – Glucose group, 54.02 ± 3.17 ng/mL in the RPG + Glucose group, and 86.31 ± 5.67 ng/mL in the RPG – Glucose group. This phenomenon can be explained by the following points: (1) GOx activity dependence: The activity of GOx is dependent on the presence of glucose. In the absence of glucose, GOx is unable to exert its catalytic effect, so the cytotoxicity of GPP is significantly reduced. (2) Cytotoxicity of Res: Res itself has a certain cytotoxicity, and Res can still have toxic effects on cells even under glucose-free conditions. Therefore, RGP still exhibits high cytotoxicity in the absence of glucose. This indicated that GOx could effectively suppress tumor cell proliferation.

Among them, the dose-dependent inhibitory trends among groups were further validated through IC_{50} analysis, with specific significant differences shown in Fig. 4d and f and the results section of the main text.

4.8. ROS

Although tumor cells have evolved metabolism to resist oxidative stress, they can still cause damage and death when ROS accumulates in large quantities [29]. The ROS surge can lead to misfolding and translocation of endoplasmic reticulum proteins in tumor cells, which are the basis for induction of ICD. As shown in Fig. 5a, b and 5c, the qualitative and quantitative characterization of ROS generation in CT26 cells were induced by the control group, GPP NMs, RPP NMs and RPG NMs groups, respectively. The cells in the GPP NMs and RPP NMs groups produced significantly stronger ROS fluorescence than those in the control group. In addition, RPG NMs induced the strongest ROS fluorescence in tumor cells, which was significantly greater than that in the control group. In RPG NMs, Res promoted ROS generation through mitochondrial regulation. Res inhibits mitochondrial electron transport chain (ETC) Complexes I and III, increasing electron leakage and resulting in substantial accumulation of ROS, including superoxide anions ($O_2^{\bullet -}$) [30,31]. Also, GOx executed a catalytic reaction within cells, promoting additional H_2O_2 production. Therefore, RPG NMs could induce a large amount of ROS in tumor cells, providing a chemical basis for the occurrence of ICD.

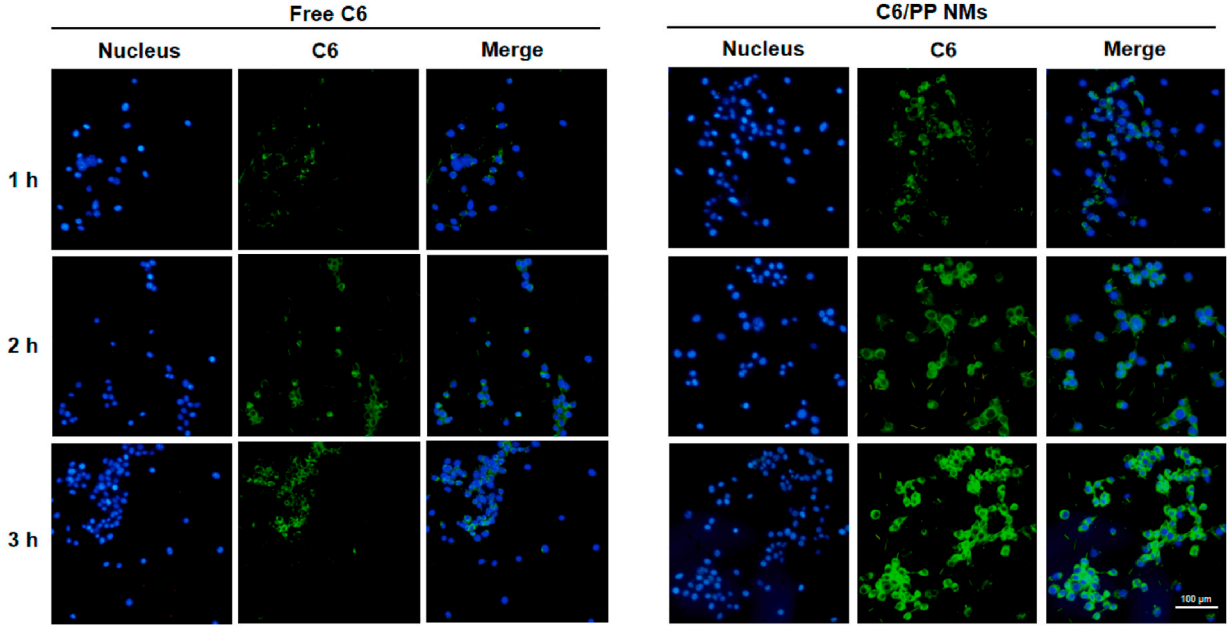

Fig. 3. Uptake fluorescence images of Free C6 and C6/PP NMs at 1 h, 2 h and 3 h (scale bar = 100 μm).

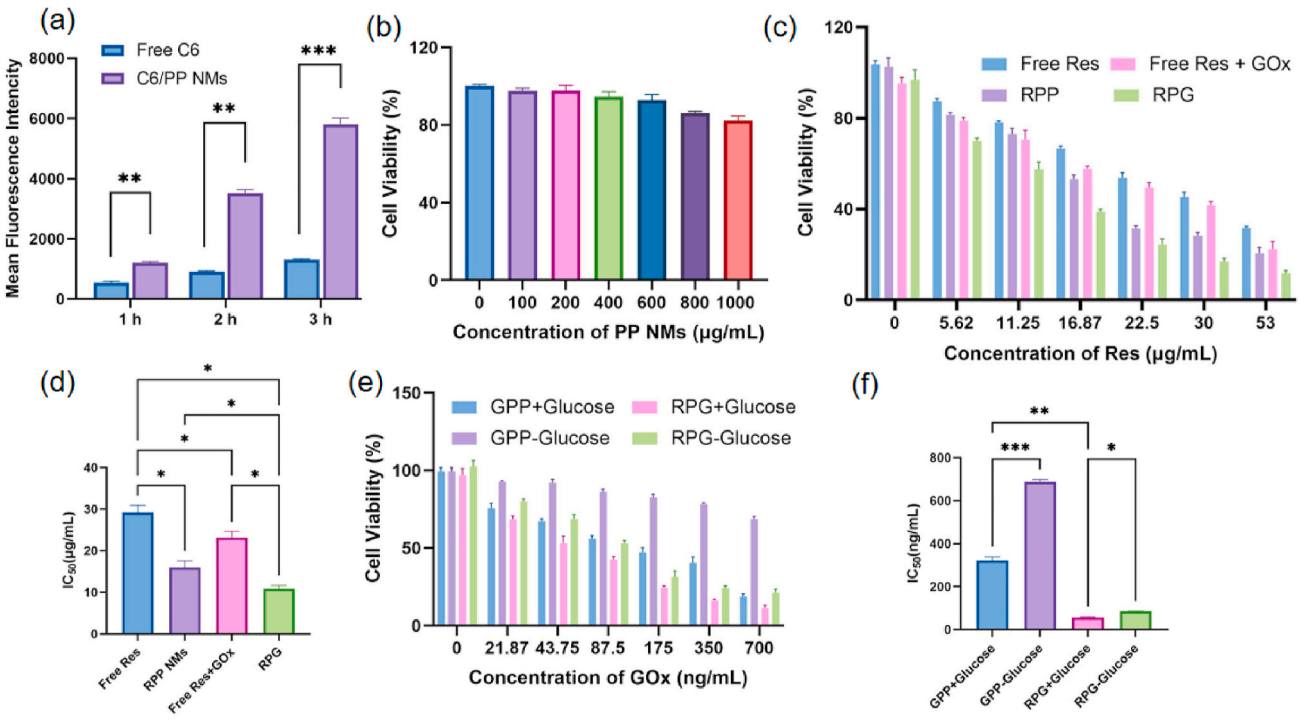

Fig. 4. (a) The uptake results of C6/PPNMs and Free C6 by CT26 cells, (b) the cytotoxicity of PP NMs as a blank carrier to CT26 cells, (c) the cell viability of Free Res, Free Res + GOx, RPP and RPG NMs groups, (d) the IC_{50} of CT26 cells, in the Res concentration, (e) cytotoxicity of each preparation group when GOx was used as the concentration, and (f) IC_{50} of CT26 cells when GOx was used as the concentration. n = 3, one way ANOVA. The data are expressed as the mean ± SD, $^{*}p < 0.05$, $^{**}p < 0.01$, $^{***}p < 0.001$.

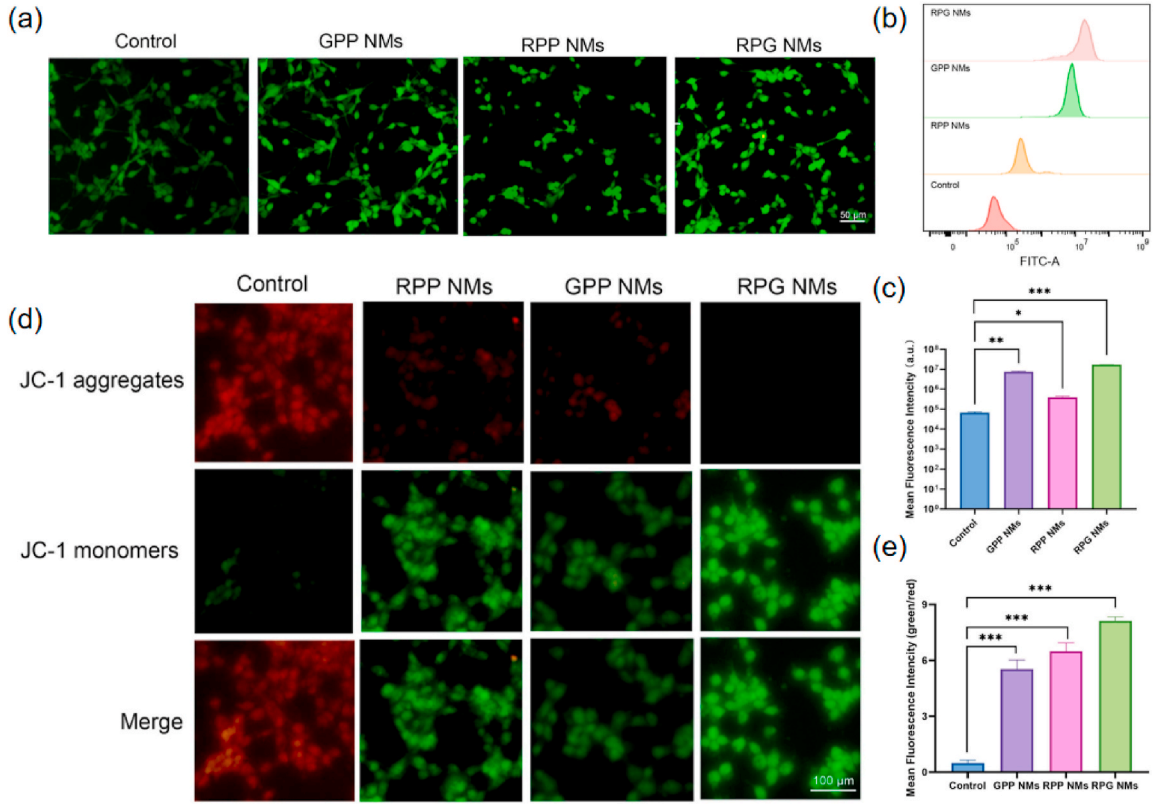

Fig. 5. (a) ROS fluorescence images with different interventions, (b) and (c) are quantitative analyses of ROS generation, (d) ΔΨm fluorescence images with different interventions, and (e) semi-quantitative analysis of ΔΨm measurements. n = 3, one way ANOVA. The data are expressed as the mean ± SD, $^{*}p < 0.05$, $^{**}p < 0.01$, $^{***}p < 0.001$.

4.9. Mitochondrial membrane potential (△Ψm)

In mitochondria, the electron transport chain generates a proton gradient through a redox reaction that drives the synthesis of ATP [32]. The stability of ΔΨm is related to the energy supply of cells and their survival state. At high ΔΨm, JC-1 molecules aggregate in mitochondria and fluoresce red. However, at low ΔΨm, green fluorescence is emitted [33]. As shown in Fig. 5d and e, △Ψm was significantly lower in GPP, RPP and RPG NMs groups than in the control group. Among them, the decrease in ΔΨm was the strongest in the RPG NMs group, showing excellent potential for mitochondrial inhibition. The decrease in ΔΨm was followed by the RPP NMs group. Res can reduce mitochondrial DNA content by depleting the ATPase 8 in tumor cells, causing mitochondrial dysfunction and decreasing ΔΨm [34]. Therefore, the decrease in ΔΨm caused by RPP was more significant than GPP. Similarly, tumor cells intervened in the RPG NMs group could accumulate much ROS, achieving a significant decrease in ΔΨm and causing the death of a large number of tumor cells.

4.10. ICD inducibility

4.10.1. The release of ATP and HMGB1

ICD primarily rely on DAMPs such as ATP, CRT, and HMGB1 and significantly enhance the immunogenicity of these dying tumor cells [35]. ATP can be released by endocytosis of ATP-containing vesicles in the ANNexin channel when tumor cells develop ICD [36]. At this point, extracellular ATP recruit myeloid cells to the active ICD site by releasing a "Find-me" signal to DC precursor cells and macrophages via the purinergic receptor P2RY2 [37]. Moreover, ICD can release HMGB1, which further strengthens the immune response. In Fig. 6a, RPG NMs induced tumor cells with the largest release of ATP (671.0 ± 10.54 μM) compared to the control group. In Fig. 6b, RPG NMs contributed to the highest levels of HMGB1 release (4164 ± 75.45 pg/mL). Similarly, other studies have shown that Res can induce ICD effects in human and mouse ovarian cancer cells [38]. Also, GOx can induce ICD effects in tumor cells in vivo and improve immunogenicity [39]. Therefore, the RPG group has the potential to induce high levels of ICD in tumor cells and improve the immunogenicity of tumor tissues.

4.10.2. Expression of CRT and determination of DCs maturity

CRT is exposed to the surface of tumor cell membranes and as a "eat me" signal, promoting its phagocytosis by immune cells such as DCs [40]. Surface-exposed CRT can bind to CD91 on the surface of antigen-presenting cells, activating both innate and adaptive immunity. In Fig. 6c–d, the expression of CRT in the cell membrane of the RPP vs. GPP NMs group showed only a small amount of fluorescence. Compared with the GPP group, CRT expressed on the surface of tumor cell membrane reached the highest fluorescence intensity after RPG NMs intervention.

CRT as DAMPs can induce maturation of DCs. In Fig. 7a–b, CD80 and CD86 positive cells are markers of mature DCs. Compared with the control group (2.86 %), RPG NMs-induced tumor cell debris significantly increased the maturity of DCs, up to 57.8 %. The GPP and RPG NMs groups reached 35.5 % and 39.7 %, respectively. Intratumoral DCs can both provide survival signals to afferent T cells and drive effector differentiation, thereby enhancing local anti-tumor immunity [41]. However, the deficiency of DCs in vivo or the expression of their immunomodulatory molecules often limits the response of anti-tumor T cells [42]. RPG NMs can induce tumor cells to release DAMPs and antigen signals, activate and recruit more DCs. DCs play a central role in

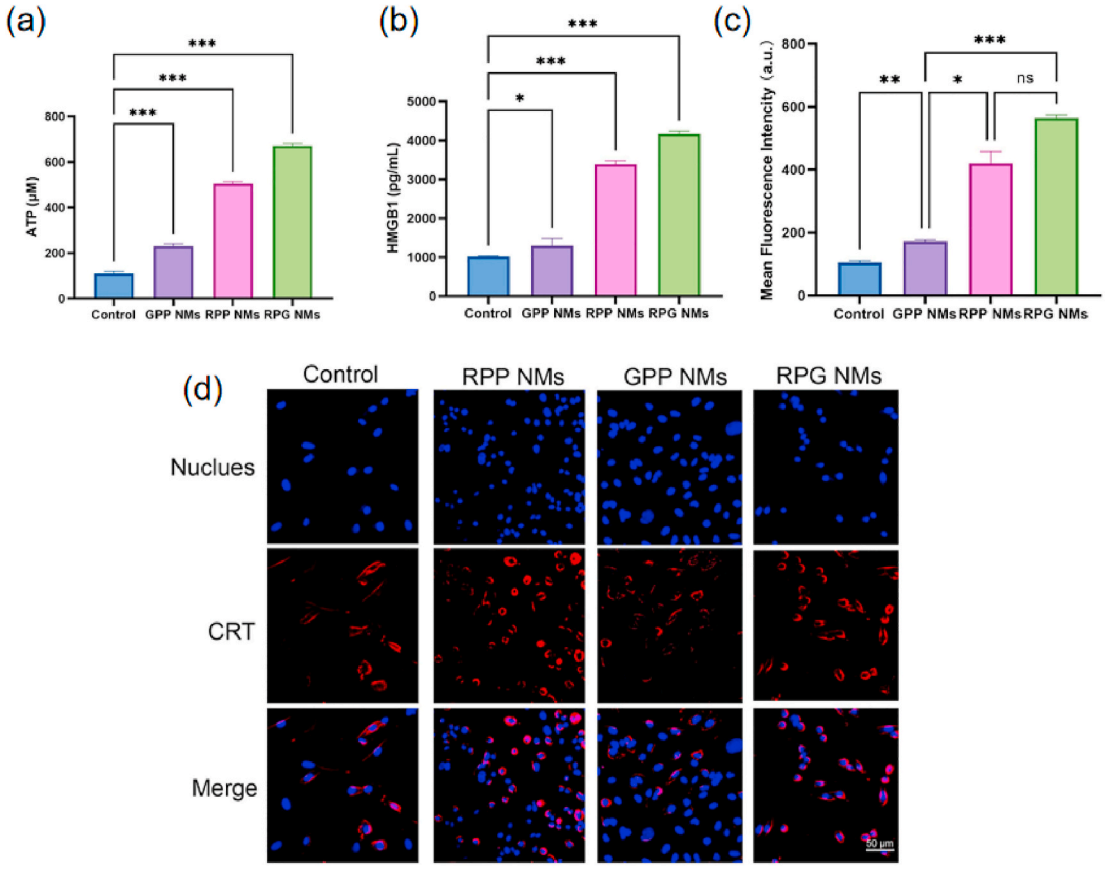

Fig. 6. (a) The levels of ATP released from tumor cells induced by different groups, (b) the levels of HMGB1 released from tumor cells induced by various preparation groups, (c) and (d) are the qualitative and quantitative analysis of CRT expression on CT26 cells induced by diverse groups. n = 3, one way ANOVA. The data are expressed as the mean ± SD, $^{*}p < 0.05$, $^{**}p < 0.01$, $^{***}p < 0.001$.

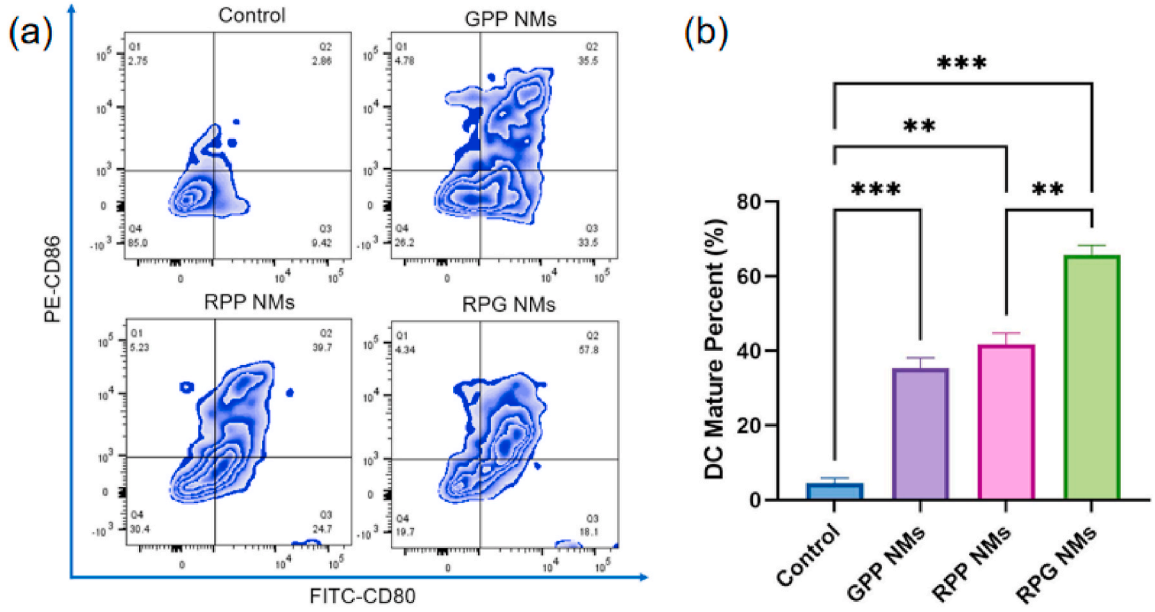

Fig. 7. (a) Flow plots for determining the maturity of DCs and (b) the maturity of induced DCs after ICD induction in tumor cells by different interventions. n = 3, one way ANOVA. The data are expressed as the mean ± SD, $*p < 0.05$, $**p < 0.01$, $***p < 0.001$.

the initiation and maintenance of anti-tumor T cell immunity. When the tumor cells are processed into DAMPs, the DC cells gradually mature and migrate to the lymph nodes. Thereafter, tumor antigens are processed and loaded onto histocompatibility complexes and presented to $CD8^+$ T cells, ultimately destroying residual tumor cells [43–46]. Therefore, the ICD effect induced by RPG NMs can not only enhance the immunogenicity of tumor cells and make tumor cells a "therapeutic vaccine", but also improve the efficacy of DCs-based tumor vaccines.

5. Conclusions

In conclusion, we have successfully designed RPG NMs for ICD induction in cancer cells by co-delivery of GOx and Res. Among them, PP copolymer can load hydrophobic Res and adsorb GOx by electrostatic interaction to achieve high drug loading and dimensional stability. RPG NMs have good monodispersity and concentrated particle size distribution, and qualified stability and biological safety. They can ensure the catalytic activity and stability of GOx and provide the basis for its function in cells. GOx in RPG NMs accelerated the rate of Res release from micelles at simulated tumor acidity. RPG NMs can significantly inhibit the viability of tumor cells. GOx can produce abundant ROS and assist Res to induce ICD in tumor cells, releasing HMGB1 and ATP. Meanwhile, RPG NMs can promote the translocation of CRT to the membrane surface of tumor cells, displaying the "eat me" signal. Interestingly, RPG NMs induced tumor cells and debris significantly enhanced the maturation of DCs. Therefore, this micelle may be a promising nanoplatform with the promise of activating tumor immune presentation functions and improving immunotherapy efficacy.

CRediT authorship contribution statement

Yuhan Fu: Writing – review & editing, Writing – original draft. **Sisi Yan:** Data curation. **Jialin Sun:** Funding acquisition. **Jianchang Huang:** Methodology. **Chunyu Yang:** Funding acquisition. **Weinan Li:** Visualization. **Yanhong Wang:** Visualization, Supervision.

Availability of data and materials

Not applicable.

Funding and acknowledgments

This work was supported by the Heilongjiang University of Chinese Medicine graduate innovative research project [No. 2023yjscx011], Genertec Medical Scienticfic Research Fund [TYYLKYJJ- 2024–040], and the Heilongjiang Touyan Innovation Team Program.

Declaration of competing interest

The authors declare that they have no known competing financial interests or personal relationships that could have appeared to influence the work reported in this paper.

Data availability

Data will be made available on request.

References

[1] A.R. Sánchez-Paulete, F.J. Cueto, M. Martínez-López, S. Labiano, A. Morales-Kastresana, M.E. Rodríguez-Ruiz, M. Jure-Kunkel, A. Azpilikueta, M.A. Aznar, J. I. Quetglas, D. Sancho, I. Melero, Cancer immunotherapy with immunomodulatory Anti-CD137 and Anti-PD-1 monoclonal antibodies requires BATF3-Dependent dendritic cells, Cancer Discov. 6 (1) (2016 Jan) 71–79.
[2] A.J. Schoenfeld, M.D. Hellmann, Acquired resistance to immune checkpoint inhibitors, Cancer Cell 37 (4) (2020 Apr 13) 443–455.
[3] Y. Li, X. Liu, X. Zhang, W. Pan, N. Li, B. Tang, Immunogenic cell death inducers for enhanced cancer immunotherapy, Chem. Commun. 57 (91) (2021 Nov 16) 12087–12097.
[4] E.W. Roberts, M.L. Broz, M. Binnewies, M.B. Headley, A.E. Nelson, D.M. Wolf, T. Kaisho, D. Bogunovic, N. Bhardwaj, M.F. Krummel, Critical role for CD103(+)/CD141(+) dendritic cells bearing CCR7 for tumor antigen trafficking and priming of T cell immunity in melanoma, Cancer Cell 30 (2) (2016 Aug 8) 324–336.
[5] J. Li, S. Zhou, J. Yu, W. Cai, Y. Yang, X. Kuang, H. Liu, Z. He, Y. Wang, Low dose shikonin and anthracyclines coloaded liposomes induce robust immunogenetic cell death for synergistic chemo-immunotherapy, J. Contr. Release 335 (2021 Jul 10) 306–319.
[6] F. Zhou, B. Feng, H. Yu, D. Wang, T. Wang, Y. Ma, S. Wang, Y. Li, Tumor microenvironment-activatable prodrug vesicles for nanoenabled cancer chemoimmunotherapy combining immunogenic cell death induction and CD47 blockade, Adv. Mater. 31 (14) (2019 Apr) e1805888.
[7] W. Yang, G. Zhu, S. Wang, G. Yu, Z. Yang, L. Lin, Z. Zhou, Y. Liu, Y. Dai, F. Zhang, Z. Shen, Y. Liu, Z. He, J. Lau, G. Niu, D.O. Kiesewetter, S. Hu, X. Chen, In situ dendritic cell vaccine for effective cancer immunotherapy, ACS Nano 13 (3) (2019 Mar 26) 3083–3094.
[8] F. Sun, Q. Zhu, T. Li, M. Saeed, Z. Xu, F. Zhong, R. Song, M. Huai, M. Zheng, C. Xie, L. Xu, H. Yu, Regulating glucose metabolism with prodrug nanoparticles for

promoting photoimmunotherapy of pancreatic cancer, Adv. Sci. (Weinh.) 8 (4) (2021 Jan 4) 2002746.
[9] H. Deng, Z. Zhou, W. Yang, L.S. Lin, S. Wang, G. Niu, J. Song, X. Chen, Endoplasmic reticulum targeting to amplify immunogenic cell death for cancer immunotherapy, Nano Lett. 20 (3) (2020 Mar 11) 1928–1933.
[10] Y. Fu, J. Sun, C. Yang, W. Li, Y. Wang, Diversified nanocarrier design to optimize glucose oxidase-mediated anti-tumor therapy: strategy and progress, Int. J. Biol. Macromol. (2025). Published online February 27.
[11] D.V. Krysko, A.D. Garg, A. Kaczmarek, O. Krysko, P. Agostinis, P. Vandenabeele, Immunogenic cell death and DAMPs in cancer therapy, Nat. Rev. Cancer 12 (12) (2012 Dec) 860–875.
[12] Y. Zhang, S. Yang, Y. Yang, T. Liu, Resveratrol induces immunogenic cell death of human and murine ovarian carcinoma cells, Infect. Agents Cancer 14 (2019) 27. Published 2019 Oct 18.
[13] J.C. Liu, D. Wang, E. Callen, C. Chen, S. Noriega, Y. Shang, D. Schürmann, Y. Song, G.N. Ramadoss, R. Chari, N. Wong, Y. Zhao, Y. He, P.D. Aplan, M.E. Ward, N. Heintz, A. Rao, P.J. McKinnon, K.W. Caldecott, P. Schär, F.L. Meng, F. Livak, W. Wu, A. Nussenzweig, Mechanism of cytarabine-induced neurotoxicity, Nature (2025 Jun 25).
[14] Y. Zhong, Z. Qiu, Y. Li, J. Huang, Z. Lu, R. Kong, et al., Nutrients deprivation of biomimetic nanozymes for Cascade catalysis triggered and oxidative damage induced tumor eradication, Chin. Chem. Lett. 36 (3) (2025).
[15] B. Pelaz, C. Alexiou, R.A. Alvarez-Puebla, F. Alves, A.M. Andrews, S. Ashraf, L. P. Balogh, L. Ballerini, A. Bestetti, C. Brendel, S. Bosi, M. Carril, W.C. Chan, C. Chen, X. Chen, X. Chen, Z. Cheng, D. Cui, J. Du, C. Dullin, A. Escudero, N. Feliu, M. Gao, M. George, Y. Gogotsi, A. Grünweller, Z. Gu, N.J. Halas, N. Hampp, R. K. Hartmann, M.C. Hersam, P. Hunziker, J. Jian, X. Jiang, P. Jungebluth, P. Kadhiresan, K. Kataoka, A. Khademhosseini, J. Kopeček, N.A. Kotov, H.F. Krug, D.S. Lee, C.M. Lehr, K.W. Leong, X.J. Liang, M. Ling Lim, L.M. Liz-Marzán, X. Ma, P. Macchiarini, H. Meng, H. Möhwald, P. Mulvaney, A.E. Nel, S. Nie, P. Nordlander, T. Okano, J. Oliveira, T.H. Park, R.M. Penner, M. Prato, V. Puntes, V.M. Rotello, A. Samarakoon, R.E. Schaak, Y. Shen, S. Sjöqvist, A.G. Skirtach, M. G. Soliman, M.M. Stevens, H.W. Sung, B.Z. Tang, R. Tietze, B.N. Udugama, J. S. VanEpps, T. Weil, P.S. Weiss, I. Willner, Y. Wu, L. Yang, Z. Yue, Q. Zhang, Q. Zhang, X.E. Zhang, Y. Zhao, X. Zhou, W.J. Parak, Diverse applications of nanomedicine, ACS Nano 11 (3) (2017 Mar 28) 2313–2381.
[16] C. Shan, H. Yang, J. Song, D. Han, A. Ivaska, L. Niu, Direct electrochemistry of glucose oxidase and biosensing for glucose based on graphene, Anal. Chem. 81 (6) (2009 Mar 15) 2378–2382.
[17] L. Bao, L. Bian, M. Zhao, J. Lei, J. Wang, Synthesis and self-assembly behavior of a biodegradable and sustainable soybean oil-based copolymer nanomicelle, Nanoscale Res. Lett. 9 (1) (2014 Aug 12) 391.
[18] Y. Pan, X. Wang, Z. Yin, Synthesis and evaluation of cationic polymeric micelles as carriers of lumbrokinase for targeted thrombolysis, Asian J. Pharm. Sci. 14 (2) (2019 Mar) 144–153.
[19] X. Pang, T. Wang, D. Jiang, W. Mu, B. Zhang, N. Zhang, Functionalized docetaxel-loaded lipid-based-nanosuspensions to enhance antitumor efficacy in vivo, Int. J. Nanomed. 14 (2019 Apr 11) 2543–2555.
[20] A.B. Kayitmazer, F. Comert, H.H. Winter, P.B. Messersmith, Rheology and gelation of hyaluronic acid/chitosan coacervates, Biomolecules 12 (12) (2022 Dec 5) 1817.
[21] Y. Zhang, Y. Takahashi, S.P. Hong, F. Liu, J. Bednarska, P.S. Goff, P. Novak, A. Shevchuk, S. Gopal, I. Barozzi, L. Magnani, H. Sakai, Y. Suguru, T. Fujii, A. Erofeev, P. Gorelkin, A. Majouga, D.J. Weiss, C. Edwards, A.P. Ivanov, D. Klenerman, E.V. Sviderskaya, J.B. Edel, Y. Korchev, High-resolution label-free 3D mapping of extracellular pH of single living cells, Nat. Commun. 10 (1) (2019 Dec 6) 5610.
[22] J. Wang, L. Wang, Y. Li, X. Wang, P. Tu, Apically targeted oral micelles exhibit highly efficient intestinal uptake and oral absorption, Int. J. Nanomed. 13 (2018 Nov 26) 7997–8012.
[23] X. Sun, G. Wang, H. Zhang, S. Hu, X. Liu, J. Tang, Y. Shen, The blood clearance kinetics and pathway of polymeric micelles in cancer drug delivery, ACS Nano 12 (6) (2018 Jun 26) 6179–6192.
[24] K.J. Paz-Alfaro, Y.G. Ruiz-Granados, S. Uribe-Carvajal, J.G. Sampedro, Trehalose-mediated thermal stabilization of glucose oxidase from Aspergillus niger, J. Biotechnol. 141 (3–4) (2009 May 20) 130–136.
[25] E.R. Bérubé, M.P. Taillon, M. Furtado, F. Garofolo, Impact of sample hemolysis on drug stability in regulated bioanalysis, Bioanalysis 3 (18) (2011 Sep) 2097–2105.
[26] N.C. Hughes, N. Bajaj, J. Fan, E.Y. Wong, Assessing the matrix effects of hemolyzed samples in bioanalysis, Bioanalysis 1 (6) (2009 Sep) 1057–1066.
[27] K. Plewes, H.W.F. Kingston, A. Ghose, R.J. Maude, M.T. Herdman, S.J. Leopold, H. Ishioka, M.M.U. Hasan, M.S. Haider, S. Alam, K.A. Piera, P. Charunwatthana, K. Silamut, T.W. Yeo, M.A. Faiz, S.J. Lee, M. Mukaka, G.D.H. Turner, N.M. Anstey, L. Jackson Roberts 2nd, N.J. White, N.P.J. Day, M.A. Hossain, A.M. Dondorp, Cell-free hemoglobin mediated oxidative stress is associated with acute kidney injury and renal replacement therapy in severe falciparum malaria: an observational study, BMC Infect. Dis. 17 (1) (2017 Apr 27) 313.
[28] M. Yuan, Y. Yang, Y. Li, Z. Yan, C. Lin, J. Chen, Mucin-like domain of mucosal addressin cell adhesion Molecule-1 facilitates integrin α4β7-Mediated cell adhesion through electrostatic repulsion, Front. Cell Dev. Biol. 8 (2020 Dec 14) 603148.
[29] G. Ong, S.E. Logue, Unfolding the interactions between endoplasmic reticulum stress and oxidative stress, Antioxidants 12 (5) (2023 Apr 22) 981.
[30] F. Oppedisano, J. Maiuolo, M. Gliozzi, V. Musolino, C. Carresi, S. Nucera, M. Scicchitano, F. Scarano, F. Bosco, R. Macrì, S. Ruga, M.C. Zito, E. Palma, C. Muscoli, V. Mollace, The potential for natural antioxidant supplementation in the early stages of neurodegenerative disorders, Int. J. Mol. Sci. 21 (7) (2020 Apr 9) 2618.
[31] Y. Luo, X. He, Q. Du, et al., Metal-based smart nanosystems in cancer immunotherapy, Explorations 4 (6) (2024) 20230134. Published 2024 Mar 22.
[32] W. Nedel, N.R. Strogulski, A. Kopczynski, L.V. Portela, Assessment of mitochondrial function and its prognostic role in sepsis: a literature review, Intensive Care Med. Exp. 12 (1) (2024 Nov 25) 107.
[33] L.D. Zorova, V.A. Popkov, E.Y. Plotnikov, D.N. Silachev, I.B. Pevzner, S. S. Jankauskas, V.A. Babenko, S.D. Zorov, A.V. Balakireva, M. Juhaszova, S. J. Sollott, D.B. Zorov, Mitochondrial membrane potential, Anal. Biochem. 552 (2018 Jul 1) 50–59.
[34] V. Prabhu, P. Srivastava, N. Yadav, M. Amadori, A. Schneider, A. Seshadri, J. Pitarresi, R. Scott, H. Zhang, S. Koochekpour, R. Gogada, D. Chandra, Resveratrol depletes mitochondrial DNA and inhibition of autophagy enhances resveratrol-induced caspase activation, Mitochondrion 13 (5) (2013 Sep) 493–499.
[35] A. Ahmed, S.W.G. Tait, Targeting immunogenic cell death in cancer, Mol. Oncol. 14 (12) (2020 Dec) 2994–3006.
[36] R. Alzeibak, T.A. Mishchenko, N.Y. Shilyagina, I.V. Balalaeva, M.V. Vedunova, D. V. Krysko, Targeting immunogenic cancer cell death by photodynamic therapy: past, present and future [published correction appears in J immunother cancer. 2021 Oct;9(10):], J. Immunother. Cancer 9 (1) (2021) e001926.
[37] Z. Li, X. Lai, S. Fu, L. Ren, H. Cai, H. Zhang, Z. Gu, X. Ma, K. Luo, Immunogenic cell death activates the tumor immune microenvironment to boost the immunotherapy efficiency, Adv. Sci. (Weinh.) 9 (22) (2022 Aug) e2201734.
[38] Y. Zhang, S. Yang, Y. Yang, T. Liu, Resveratrol induces immunogenic cell death of human and murine ovarian carcinoma cells, Infect. Agents Cancer 14 (2019 Oct 18) 27.
[39] S. Jafari, S. Heydarian, R. Lai, E. Mehdizadeh Aghdam, O. Molavi, Silibinin induces immunogenic cell death in cancer cells and enhances the induced immunogenicity by chemotherapy, Bioimpacts 13 (1) (2023) 51–61.
[40] L. Galluzzi, I. Vitale, S. Warren, et al., Consensus guidelines for the definition, detection and interpretation of immunogenic cell death [published correction appears in J immunother cancer. 2020 May;8(1), J. Immunother. Cancer 8 (1) (2020) e000337.
[41] S. Jhunjhunwala, C. Hammer, L. Delamarre, Antigen presentation in cancer: insights into tumour immunogenicity and immune evasion, Nat. Rev. Cancer 21 (5) (2021 May) 298–312.
[42] Q. Yu, Y. Dong, X. Wang, C. Su, R. Zhang, W. Xu, S. Jiang, Y. Dang, W. Jiang, Pharmacological induction of MHC-I expression in tumor cells revitalizes T cell antitumor immunity, JCI Insight 9 (17) (2024 Aug 6) e177788.
[43] H. Matsushita, M.D. Vesely, D.C. Koboldt, C.G. Rickert, R. Uppaluri, V.J. Magrini, C.D. Arthur, J.M. White, Y.S. Chen, L.K. Shea, J. Hundal, M.C. Wendl, R. Demeter, T. Wylie, J.P. Allison, M.J. Smyth, L.J. Old, E.R. Mardis, R.D. Schreiber, Cancer exome analysis reveals a T-cell-dependent mechanism of cancer immunoediting, Nature 482 (7385) (2012 Feb 8) 400–404.
[44] L. Bai, J. Yang, S. Yu, Z. Xiang, Y. Zeng, M. Shen, X. Kou, Q. Wu, C. Gong, Self-sufficient nanoparticles with dual-enzyme activity trigger radical storms and activate cascade-amplified antitumor immunologic responses, Acta Pharm. Sin. B 14 (2) (2024 Feb) 821–835.
[45] S. Zhou, Y. Li, R. Wu, T. Chen, Y. Xu, H. Le, et al., A multifunctional nutrient transfer nanocrispr scaffold induces metabolic remodeling to fuel cancer immunotherapy, Nano Today 58 (000) (2024).
[46] C. Ou, M. Xiao, X. Zheng, X. Huang, S. Yang, Y. Leng, X. Liu, X. Liang, L. Song, Y. You, S. Yao, C. Gong, Programmable double-unlock nanocomplex self-supplies phenylalanine ammonia-lyase for precise phenylalanine deprivation of tumors, Chin. Chem. Lett. 35 (8) (2024) 109275.